Pellet-Model Effects on Simulation Models for Fixed-Bed Desulfurization Reactors

Detailed mathematical models, pore or grain based, describing diffusion, reaction, and pore structure evolution in pellets of porous solids are used to simulate, along with a macroscopic reactor design model, the transient phenomena that take place during desulfurization of coal gas in fixed-bed reactors of pellets of metal oxide sorbents. Our computer simulation results show that the form of the pore- or grain-size distribution strongly influences the predictions of the overall reactor design model.

Stratis V. Sotirchos
Solon Zarkanitis
Department of Chemical Engineering
University of Rochester
Rochester, NY 14627

Introduction

Hot coal gas desulfurization processes are based on the capacity of various metal/metal oxide solids to react with hydrogen sulfide and other sulfur-containing compounds to form metal sulfides. The economic feasibility of a given metal/metal oxide sorbent depends largely on its regeneration characteristics. For most metal/metal oxide solids, regeneration is carried out by heating the spent sorbent (metal sulfide) in air or air/stream mixtures (Tamhankar, 1982). An economically feasible desulfurization sorbent should not only be regenerable but also retain its original sulfur capture capacity over a number of absorptive/regenerative cycles. Various supported (on ceramic support) or unsupported metal/metal oxide sorbents have been studied experimentally for hot gas desulfurization, such as iron oxides, zinc oxide, copper/copper oxides, nickel, and cobalt titanate [for example, see studies by Gibson and Harrison (1980), Tamhankar et al. (1981), Ranade and Harrison (1981), Gaillet and Harrison (1982), Jalan (1983), and Anderson et al. (1984)]. Iron oxide, zinc oxide, and copper/copper oxide based systems have attracted the most interest as they appear to be the most promising ones.

Both the sulfur absorption and sorbent regeneration steps are noncatalytic gas-solid reactions characterized by formation of a solid product. The solids used in hot gas desulfurization are highly porous, and consequently reaction occurs mainly in the interior of the solid pellets at the interface between solid reactant and solid product. Because of the formation of the solid product, a number of processes must be considered in the development of single-pellet models for the above gas-solid systems and in the analysis of obtained experimental data, in addition to intraparticle diffusion and reaction. The internal structure of the reacting solid, for instance, must be described by two temporally and spatially evolving surfaces, the reaction surface (solid reactant-solid product interface) and the pore surface. Moreover, because of slow diffusion of the reactive species in the produce layer, large concentration gradients may be present in the product layer even if appreciable concentration gradients do not exist in the porous structure.

The presence of the solid product may lead to additional complications if the ratio of stoichiometrically equivalent volumes of solid reactant and solid product is greater than one, as it appears to be the case with most metal oxide sorbents used in hot gas desulfurization. Since the solid product occupies more space than the solid from which it results, the porosity diminishes with the progress of the reaction, and incomplete conversion and pore plugging phenomena might be observed. Under conditions of significant concentration gradients in the interior of the reacting particles or pellets, pore closure may first occur at the external surface preventing further penetration of the reactive gases and subsequent reaction in the interior. Another phenomenon that may take place in noncatalytic gas-solid systems exhibiting pore closure behavior is the formation of inaccessible pore space. This situation results when the feeder pores of a finite cluster of pores are filled with solid product.

Generalized pore and grain structural models were developed by our research group (Sotirchos and Yu, 1985, 1988; Yu and Sotirchos, 1987) for application to gas-solid reactions with or without pore closure behavior. Application of these models to limestone sulfation showed that the behavior of the reacting porous particles is influenced strongly by the form of their pore size distribution. Under strong intraparticle diffusional limitations, the pore size distribution was found to determine not only the overall reaction rate but also the maximum conversion (sorptive capacity) reached by the system. The predictions of our mathe-

Correspondence concerning this paper should be addressed to S. V. Sotirchos.

matical models were verified by carrying out reactivity experiments on the reaction of calcined limestone with SO_2 (Yu, 1987). The conclusions of the above studies are expected to be directly applicable to hot gas desulfurization sorbents since they may also exhibit pore closure behavior. Moreover, past experimental studies have revealed strong effects of pellet size on the sorptive capacity of desulfurization sorbents [e.g., Jalan (1983) for the CuO/ZnO sorbent] suggesting that the process occurs under conditions of significant intraparticle concentration gradients.

A detailed mathematical model is presented in this study for the description of the dynamic behavior of fixed-bed reactors used for desulfurization of coal gas at high temperatures. Structural models of varying complexity and rigor, pore or grain based, are used to follow the evolution of the properties of the pore structure in the interior of the metal oxide pellets with the extent of the reaction. These structural models are based on the generalized random pore and grain models that have been developed by Sotirchos and Yu (1985, 1988) for gas-solid reactions with solid product. The desulfurization model is applied to the analysis of the transient behavior of fixed-bed reactors loaded with pellets of zinc oxide. Particular emphasis is placed on the investigation of the effects of the structural model used for representation of the pore structure of the pellets, as well as of the effects of the structural characteristics of the porous solid (internal surface area, porosity, and pore size distribution), on the breakthrough behavior of the reactor and, hence, on the utilization of the sorbent.

Development of the Mathematical Models

We consider a fixed-bed reactor packed with porous pellets consisting of metal oxide $M_{\nu_a} O_{\nu_b}$ and inert solid species. The coal gas entering the chemical reactor is treated as a dilute mixture of H_2S, which is assumed to be the primary contaminant. The existence of other sulfur-containing compounds in the coal gas is disregarded in the present analysis. The other gaseous species contained in the mixture are carbon monoxide, methane, hydrogen, carbon dioxide, nitrogen, and other organic compounds present at low concentrations. With the exception of H_2S which is assumed to react with the metal oxide according to the reaction equation

$$M_{\nu_a}O_{\nu_b} + \nu_b H_2S \rightarrow M_{\nu_a}S_{\nu_b} + \nu_b H_2O \qquad (1)$$

all other chemical species are considered to be inert with respect to it. With regard to our application, therefore, the coal gas can be treated as a pseudobinary mixture of hydrogen sulfide and of an inert gaseous 'species.'

Because of the presence of small concentrations of gaseous reactant (H_2S) in the reactive mixture entering the chemical reactor, relatively low amounts of heat are released during the chemical reaction, and as a result, heat effects associated with the occurrence of the desulfurization reaction can be neglected, and the fixed-bed reactor and the porous pellets may be treated as isothermal. The mathematical model for the reactor system, therefore, consists of equations describing the convective and diffusive transport of the gaseous reactant in the void space of the bed and the variation of the local average conversion of the solid with the position in the reactor, equations describing the diffusion of the gaseous species in the interior of each pellet, and finally equations describing the temporal and spatial evolution of the structural properties of the porous structure and of the conversion of the solid reactant in the interior of the pellets.

Equations for the fixed-bed

The material balance of hydrogen sulfide in the fixed-bed expressed in terms of its concentration, c_f, is written in the presence of mixing in the axial direction as (Froment and Bischoff, 1979; Lee, 1985)

$$\epsilon_b \frac{\partial c_f}{\partial t} = D_b \frac{\partial^2 c_f}{\partial z^2} - u \frac{\partial c_f}{\partial z} - \nu_b(1 - \epsilon_b)\bar{R}_v \qquad (2)$$

$\bar{R}_v$ is the local reaction in the bed expressed in moles of metal oxide per unit of pellet volume and time, D_b is the axial dispersion coefficient of the gaseous reactant in the bed, ϵ_b is the porosity of the bed, and u is the superficial velocity.

The material balance for the solid reactant expressed in terms of its local average conversion in the bed, $\bar{\xi}$, is written as

$$\frac{\partial \bar{\xi}}{\partial t} = \frac{v_S}{1 - \epsilon_0}\bar{R}_v \qquad (3)$$

where ϵ_o is the initial porosity of the pellets, and v_S is the 'molar' volume of the unreacted solid phase expressed as volume of solid phase per mole of solid reactant.

The Danckwerts boundary conditions (Danckwerts, 1953) are imposed on Eq. 2, and it is assumed that the reactor is initially loaded with fresh (unreacted) pellets and that the initial concentration of the gaseous reactant is equal to zero. In mathematical form we have that:

At $z = 0$:

$$-D_b \frac{\partial c_f}{\partial z} = u(c_i - c_f) \qquad (4)$$

At $z = L$:

$$\frac{\partial c_f}{\partial z} = 0 \qquad (5)$$

At $t = 0$:

$$c_f = 0; \bar{\xi} = 0 \qquad (6a,b)$$

It is obvious from the form of Eq. 2 that ϵ_b and D_b are treated as being invariant with time, a consequence of our tacit assumption that pellet size changes occurring as a result of the chemical reaction are insignificant. The length scale over which significant concentration differences are observed along the bed is assumed to be considerably larger than the average pellet size. This assumption enables us to consider that the local average reaction rate at some point in the bed equals at all times the average reaction rate of a pellet whose ambient conditions (concentration and temperature) are identical to those at the same point of the bed. Similarly, the local average conversion of the solid at some point of the bed can be considered equal to the average conversion of a pellet located at the same position.

If the pseudosteady-state approximation is introduced in the material balance of the gaseous reactant in the interior of the pellets, the local average reaction rate in the bed, $\bar{R}_v$, for a first-

order reaction—as it is the case considered in the present study—can be related to the reactant concentration in the bed by the relation

$$\bar{R}_v = \bar{k}_v(\bar{\xi})c_f \tag{7}$$

where $\bar{k}_v(\bar{\xi})$ is a local average reaction rate constant which depends only on the local average conversion in the bed or, equivalently, on the average conversion of the pellet. The validity of Eq. 7 will become obvious after the model equations for the interior of the pellet and for the structure evolution problem are presented.

Equations for the pellets

The material balance of hydrogen sulfide in the interior of the pellets expressed in terms of its concentration, c_p, has the form

$$\frac{\partial(\epsilon_p c_p)}{\partial t} = \frac{1}{r^s}\frac{\partial}{\partial r}\left(r^s D_e \frac{\partial c_p}{\partial r}\right) - \nu_b R_v \tag{8}$$

ϵ_p is the porosity, D_e is the effective diffusivity of hydrogen sulfide in the pellet, R_v is the local reaction rate expressed as moles of solid reactant per unit of pellet volume and time, and s is the shape factor of the pellet (0 for a slab, 1 for a cylinder, and 2 for a sphere).

If the pseudosteady-state approximation is applied in the diffusion equation of the gaseous reactant through the product layer surrounding the pores of the pellet (see the following section), the effective diffusivity in the porous structure, D_e, becomes a function of the local conversion, ξ, only. Moreover, the local reaction rate, R_v, may be related to the concentration in the pores c_p, by the expression

$$R_v = k_v(\xi)c_p \tag{9}$$

where $k_v(\xi)$ is a volumetric reaction rate constant that depends only on the local conversion. The pseudosteady-state approximation is also introduced in Eq. 8 by assuming that changes occurring in the gas phase are much faster than those occurring in the porous structure of the solid. Assuming pseudosteady state and using Eq. 9, Eq. 8 becomes:

$$\frac{1}{r^s}\frac{\partial}{\partial r}\left(r^s D_e(\xi)\frac{\partial y_p}{\partial r}\right) - \nu_b k_v(\xi) y_p = 0 \tag{10}$$

The material balance for the solid expressed in terms of the local conversion, ξ, is written

$$\frac{\partial \xi}{\partial t'} = c_f^* \frac{v_S}{(1-\epsilon_o)} k_v(\xi) y_p \tag{11}$$

The following boundary and initial conditions are applied to Eqs. 8 and 11:

$r = 0$:

$$\frac{\partial y_p}{\partial r} = 0 \tag{12}$$

$r = a$:

$$-D_e \frac{\partial y_p}{\partial r} = k_g(y_p - 1) \tag{13}$$

$t' = 0$:

$$y_p = 0;\ \xi = 0 \tag{14a,b}$$

with

$$y_p = \frac{c_p}{c_f};\ t' = \frac{1}{c_f^*}\int_0^t c_f\, dt \tag{15a,b}$$

where c_f^* is a reference concentration.

It is clear from Eqs. 10–14 that the state of the reacting single pellet system is a single function of the time variable t' defined in Eq. 15b or, equivalently (as Eq. 11 implies), of the average conversion of the pellet. This approximation leads, as it will be explained in more detail later, to considerable simplification of the overall computational procedure since it enables us to solve the above set of equations independently of the equations for the fixed bed.

The average reaction rate per unit of pellet volume that is needed in the fixed-bed equations is computed by averaging Eq. 9 over the pellet volume. By doing so and using Eq. 15a, the following expression is obtained for the average reaction rate constant of Eq. 7:

$$\bar{k}_v(\bar{\xi}) = \frac{1}{a^{s+1}}\int_0^a k_v(\xi) y_p d(r^{s+1}) \tag{16}$$

with $\bar{\xi}$ obviously given by

$$\bar{\xi} = \frac{1}{a^{s+1}}\int_0^a \xi d(r^{s+1}) \tag{17}$$

Equations for the structure evolution problem

The structural models used in this study to describe the evolution of the porous structure of the porous sorbent in the course of its reaction with H_2S are based on the random pore and random grain models that were developed by Sotirchos and Yu (1985, 1988). A brief description of these models will be given in the following paragraphs. Readers interested in more details are advised to consult the aforementioned research articles.

The random pore models consider that the initial pore space of the fresh sorbent can be described by a population of cylindrical capillaries of distributed or uniform size that are randomly distributed in the three-dimensional space. The population of cylinders is described by the distribution density $l_o(R_o)$ where $l_o(R_o)dR_o$ is the length of pores axes per unit volume that belong to capillaries with size in the range $[R_o,\ R_o + dR_o]$. Both discrete and continuous distributions of pore size were considered by Sotirchos and Yu (1985), but in this study we consider discrete distributions of pore size only, since in this case the numerical procedure involved in the solution of the model equations is considerably simpler.

For a discrete pore size distribution involving N initial pore

sizes, $R_{o1}, R_{o2}, \ldots, R_{oN}$, we obviously have that

$$l_o(R_o) = \sum_{i=1}^{N} l_{oi}\delta(R_o - R_{oi}) \tag{18}$$

where $\delta(\cdot)$ is the delta function, and l_{oi} is the length of pore axes of pores with size R_{oi}. The length distribution density, $l_o(R_o)$, can be determined from the experimentally measured pore size distribution of the solid which for a discrete pore size system obviously has the form

$$\epsilon_o(R_o) = \sum_{i=1}^{N} \epsilon_{oi}\delta(R_o - R_{oi}) \tag{19}$$

It can be shown (Gavalas, 1980; Sotirchos and Yu, 1985) that

$$l_{oi} = \frac{1}{\pi R_{oi}^2} \ln\left[\frac{1 - \sum_{j=i+1}^{N} \epsilon_{oj}}{1 - \sum_{j=i}^{N} \epsilon_{oj}}\right] \tag{20}$$

Notice that ϵ_{oi} represents the pore volume that belongs to capillaries of size R_{oi} including the overlap value with smaller capillaries.

The random grain models (Sotirchos and Yu, 1988) consider that the solid phase of the unreacted sorbent can be described by a population of grains (plate-like, cylindrical, or spherical) of distributed or uniform size which are randomly distributed in the three-dimensional space. The population of grains is described by the distribution density $n_o(R_o)$ where $n_o(R_o)dR_o$ is the number of grains per unit volume with size in the range $[R_o, R_o + dR_o]$. We consider cylindrical grains of average length $\bar{L}$ and slab grains of average surface area $\bar{A}$, where $\bar{L}$ and $\bar{A}$ are chosen arbitrarily. As in the case of the random pore models, in this study we will consider structures described by discrete grain size distributions. It is shown (Sotirchos and Yu, 1988) that the number density function

$$n_o(R_o) = \sum_{i=1}^{N} n_{oi}\delta(R_o - R_{oi}) \tag{21}$$

is related to the distribution density of the volume fraction of the solid phase

$$\phi_o(R_o) = \sum_{i=1}^{N} \phi_{oi}\delta(R_o - R_{oi}) \tag{22}$$

by the expression

$$n_{oi} = \frac{1}{fR_o^{s+1}} \ln\left[\frac{1 - \sum_{j=i+1}^{N} \phi_{oj}}{1 - \sum_{j=i}^{N} \phi_{oj}}\right] \tag{23}$$

ϕ_{oi} is the volume fraction of the solid phase that belong to grains with size R_{oi} including the overlapping volume with smaller grains, s is the shape factor of the grains, and f is their geometric factor ($4\pi/3$ for spheres, $\pi\bar{L}$ for cylinders, and $2\bar{A}$ for slabs).

After the metal oxide contained in the sorbent starts reacting with hydrogen sulfide, each pore or grain considered in the initial pore structure is covered by a layer of solid product, and the internal structure of the solid is, therefore, described by two receding surfaces defining the reacted solid-gas interface (pore surface) and the reacted-unreacted solid interface (reaction surface). In order to simplify the analysis of the pore structure problem, we assume that points of the reaction surface or of the pore surface of the same radius of curvature move with the same velocity (Sotirchos and Yu, 1985). Because of the above assumptions, the reaction and pore surfaces of the reacting structure can be described by populations of entities (pores or grains, depending on which model is used) that are concentric to (spheres), coaxial to (cylinders), or have the same plane of symmetry (plates) as the entities used to represent the original structure. An entity of initial size R_{oi}, therefore, gives rise to two entities, one with size $R_{ri}(t)$ that is used to represent the reaction surface and one with size $R_{pi}(t)$ that represents the pore surface.

For grain structures R_{ri} represents the size of the unreacted core of the grain which obviously decreases monotonically with the conversion, and as a result, the unreacted core of a grain may vanish at some time instant. The unreacted cores of different size grains vanish at different times, with the cores of the smallest size grains vanishing first. For pore structures, R_{pi} represents the size of the capillary used to represent the pore structure of the porous medium which may increase or decrease with time depending on the stoichiometric volume ratio of the solid product-solid reactant system, $Z = v_P/v_S$, where v_P is the 'molar' volume of the reacted sorbent phase expressed as volume per mole of product. Obviously, for Z greater than 1.0 the produced solid product occupies more space than the solid reactant it replaces, and consequently R_{pi} increases with time, while the porosity of the solid decreases. It is assumed that a pore is completely plugged with solid product when its size reaches a critical threshold value, R_{pc}. Let ϵ_p be the porosity of the porous structure, and ϵ_r be the 'porosity' of the reaction surface structure, i.e., the volume fraction of void and reacted phases. The conversion of the solid is related to ϵ_p and ϵ_r by the relation

$$\xi = \frac{\epsilon_o - \epsilon_p}{(Z-1)(1-\epsilon_o)} = \frac{\epsilon_r - \epsilon_o}{1 - \epsilon_o} \tag{24a}$$

$$\epsilon_r = \epsilon_o + (\epsilon_o - \epsilon_p)/(Z-1) \tag{24b}$$

By setting $\epsilon_p = 0$ in Eq. 24a, one can find whether for given values of initial porosity and stoichiometric value ratio, complete pore closure may take place before complete conversion is reached.

Equations for Distributed Pore Growth. The equations for the variation of R_{ri} and R_{pi} with time are derived by solving the pseudosteady state diffusion equation of H_2S in the product layer surrounding pores of initial radius R_{oi} and by performing a mass balance on the solid material. For a first order reaction with intrinsic reaction rate given by $R_s = k_s c_{H_2S}$, we have that (Sotirchos and Yu, 1985, 1988)

$$\frac{dR_{ri}}{dt} = \frac{\lambda v_S k_s c_p}{1 + \frac{v_b k_s}{D_p} g_i} \tag{25}$$

$$\frac{dR_{pi}}{dt} = -\frac{dR_{ri}}{dt}\left[(Z-1)\frac{\sigma_{ri}}{\sigma_{pi}}\right] \tag{26}$$

with

$$\frac{dg_i}{dt} = \lambda\left[\frac{dR_{ri}}{dt} - \frac{\sigma_{ri}}{\sigma_{pi}}\frac{dR_{pi}}{dt}\right] \tag{27}$$

$$R_{pi}(0) = R_{ri}(0) = R_{oi};\ g_i = 0 \tag{28a,b,c}$$

where

$$\lambda = \begin{cases} 1, & \text{for pores} \\ -1, & \text{for grains} \end{cases}$$

σ_{ri} or σ_{pi} is the reaction or pore surface area per unit volume that belongs to entities with initial size R_{oi}, and D_p is the diffusion coefficient of H_2S in the product layer. When the unreacted core of a grain vanishes or a pore becomes plugged, the rates of change of R_{pi} and R_{ri} are set equal to zero.

For pore structures σ_{ri}, σ_{pi}, ϵ_p, and ϵ_r are given by the expressions (Sotirchos and Yu, 1985)

$$\sigma_{(r,p)i} = 2\pi(1-\epsilon_{(r,p)})R_{(r,p)i}l_{oi} \tag{29}$$

$$\epsilon_{(r,p)} = 1 - \exp\left(-\pi\sum_{i=1}^{N} R_{(r,p)i}^2 l_{oi}\right) \tag{30}$$

For grain structures, on the other hand, we have that (Sotirchos and Yu, 1988)

$$\sigma_{(r,p)i} = (s+1)f\epsilon_{(r,p)}R_{(r,p)i}^s n_{oi} \tag{31}$$

$$\epsilon_{(r,p)} = \exp\left[-f\sum_{i=1}^{N} R_{(r,p)i}^{s+1} n_{oi}\right] \tag{32}$$

Notice that ϵ_r may also be computed from ϵ_p using Eq. 24b. In both cases, the reaction or pore surface area per unit volume is given by

$$S_{(r,p)} = \sum_{i=1}^{N} \sigma_{(r,p)i} \tag{33}$$

Figure 1 presents a section (1 μm × 1 μm) of a random bimodal pore structure of 250 and 500 Å pores (initial radii) at 20% conversion, generated through computer simulation (Burganos, 1988). The initial porosity of the structure of Figure 1 is 0.5, the porosities of the two families of pores are equal, and the stoichiometric volume ratio is 3. (The hatched regions represent the solid product, and the cross-hatched the solid reactant.)

Equations for R_{pi} and R_{ri} for Uniform Pore Growth. The equation for the change of R_{ri} and R_{pi} with time can be considerably simplified if one assumes that all points of the pore and reaction surfaces that belong to active pores or grains move with the same velocity. We introduce two average growth variables q_r and q_p, where

$$R_{(r,p)i} = R_o + q_{(r,p)} \tag{34}$$

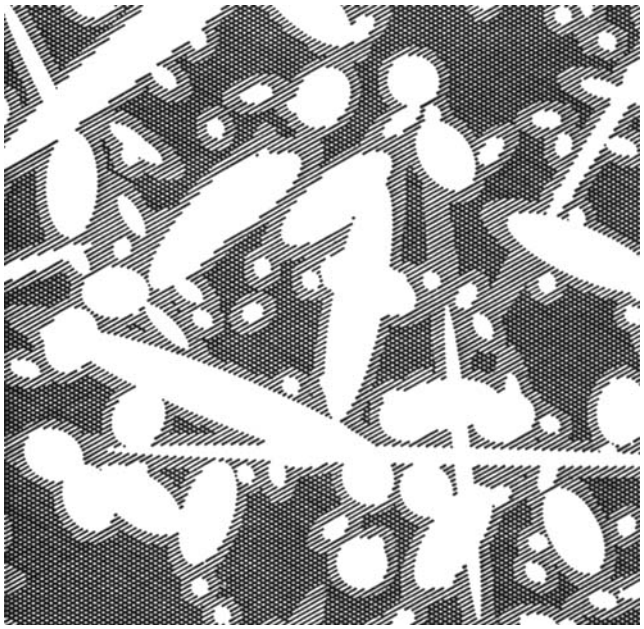

Figure 1. Computer-generated section (1 μm × 1 μm) of a random pore structure with discrete bimodal distribution of pore size.

$\xi = 0.2$; $Z = 3$; $\epsilon_o = 0.5$; $\epsilon_{ol} = 0.25$; $R_{ol} = 200$ Å; and $R_{o2} = 500$ Å. (The hatched regions represent the solid product, and the cross-hatched the solid reactant.)

The equations for the change of q_r and q_p are derived by solving the pseudosteady-state equation in the product layer of all active pores or grains and by performing a solid mass balance for all active pores or grains. We have that

$$\frac{dq_r}{dt} = \frac{\lambda v_S k_s c_p}{1 + \lambda\dfrac{v_b k_s}{D_P} S_{rm}(q_r)\displaystyle\int_{q_p}^{q_r}\frac{dq}{S_{(r,p)}(q)}} \tag{35}$$

$$\frac{dq_p}{dt} = -(Z-1)\frac{S_{rm}(q_r)}{S_{pm}(q_p)}\frac{dq_r}{dt} \tag{36}$$

with

$$q_r(0) = q_p(0) = 0 \tag{37a,b}$$

$S_{(r,p)m}(q_r)$ is the reaction or pore surface area that belongs to entities with initial size greater than or equal to R_{om}, where R_{om} is the least initial pore or grain size that is still active, i.e., the corresponding pore size is greater than the threshold for closure, R_{pc}, or the corresponding size of the unreacted core of the grain is finite. For pores, $S_{(r,p)m}(q)$ is given by

$$S_{(r,p)m}(q) = 2\pi(1-\epsilon_{(r,p)})\left(\sum_{i=m}^{N}(R_{oi}+q)l_{oi}\right) \tag{38}$$

while for grains, we have that

$$S_{(r,p)m}(q) = (s+1)f\epsilon_{(r,p)}\left(\sum_{i=m}^{N}(R_{oi}+q)^s n_{oi}\right) \tag{39}$$

Equations for D_e and k_v. The effective diffusivity for pore structures is obtained by averaging the diffusivity of H_2S in a single pore over the pore size distribution. For a discrete pore system, we have that

$$D_e = \frac{1}{\eta} \sum_{i=m}^{N} D_A(R_{pi}) \epsilon_{pi} \tag{40}$$

with

$$\frac{1}{D_A(R_p)} = \frac{1}{\mathcal{D}_{AB}} + \frac{1}{D_{KA}(R_p)} \tag{41}$$

m is the index of the least pore size that is still active, and ϵ_{pi} is the porosity of pores of size R_{pi}. The latter is given by (Sotirchos and Yu, 1985)

$$\epsilon_{pi} = \exp\left(-\pi \sum_{j=i+1}^{N} l_{oj} R_{pj}^2\right) - \exp\left(-\pi \sum_{j=i}^{N} l_{oj} R_{pj}^2\right) \tag{42}$$

For grain structures, the effective diffusivity is obtained from the expression

$$D_e = \frac{\epsilon_p}{\eta} D_A(\bar{R}_p); \quad \bar{R}_p = \frac{2\epsilon_p}{S_p} \tag{43a,b}$$

The local reaction rate is obtained by averaging the reaction rate for a point of curvature R_{ri} over all points of the reaction surface. We have that

$$R_v = \frac{\lambda}{v_S} \sum_{i=m}^{N} \left(\frac{dR_{ri}}{dt}\right) \sigma_{ri} \tag{44}$$

Using Eq. 25, or Eqs. 34 and 35, we find that

$$k_v = k_s \sum_{i=m}^{N} \frac{2\pi(1-\epsilon_r) R_{ri} l_{oi}}{1 + \lambda \dfrac{v_b k_s}{D_P} g_i} \tag{45}$$

or

$$k_v = k_s \frac{S_{rm}(q_r)}{1 + \lambda \dfrac{v_b k_s}{D_P} S_{rm}(q_r) \displaystyle\int_{q_p}^{q_r} \frac{dq_r}{S_{(r,p)m}(q)}} \tag{46}$$

It is clear from the form of Eqs. 25–27, or Eqs. 35 and 36, that the results of the structural models can be rendered independent of the concentration in the pores by defining a new time variable given by

$$t'' = \frac{1}{c_f^*} \int_0^t c_p \, dt.$$

(Compare with Eq. 15b.) Therefore, the structural properties of the solid, and consequently D_e and k_v, depend only on the conversion of the solid and not on the concentration history of the gaseous reactant.

Computational Procedure

It must have become obvious from the form of the model equations presented in the previous section that the three submodels can be solved sequentially. We first solve the structural model and form a database for the variation of $k_v(\xi)$ and $D_e(\xi)$ with the local conversion in the pellet. The solution of the model for a single pellet then follows, and this helps us to construct a database for the variation of $\bar{k}_v(\bar{\xi})$ with the average conversion in the pellet, which is then used to solve the equations for the fixed bed.

The equations for the structural model are solved using a Gear-type integrator. The equations for the single pellet and the fixed-bed model are solved using cubic B-spline collocation (de Boor, 1978) to discretize the equations in space which is followed by temporal integration using a differential-algebraic equation solver for the pellet equations and a Gear type integrator for the fixed-bed equations. The values of $k_v(\xi)$ and $D_e(\xi)$ or $\bar{k}_v(\bar{\xi})$ at a given local or average conversion value are obtained through interpolation in the appropriate database using a procedure based on 'tensioned' splines (de Boor, 1978).

Application to *ZnO* and Discussion of the Results

The mathematical model that was developed in the previous sections is used here to study the behavior of a laboratory-scale desulfurization reactor packed with ZnO pellets of spherical shape. The values of the physical, pore structure, kinetic, and fixed-bed parameters employed in our computations are given in Table 1. The space velocity corresponding to the data of Table 1 is 3,600 h^{-1}, while the Peclet number of 500 is based on an axial dispersion coefficient of 2.0×10^{-5} m^2/s. The pseudobinary diffusion coefficient of H_2S in the mixture was estimated using the Chapman-Enskog equation for a binary mixture of H_2S and N_2, while the tortuosity factor was taken equal to 3 for the cylindrical pore models (Eq. 44) and to 2 for the grain models (Eq. 43). The reaction rate constant given in Table 1 was estimated using initial reaction rate data for the ZnO–H_2S reaction reported by Westmoreland et al. (1977) for the temperature range 350–750°C. Finally, the value chosen for the solid product layer diffusivity D_P was based on values obtained by various investigators by analyzing conversion vs. time data (e.g., Christman and Edgar, 1983; Sotirchos and Yu, 1985) for the diffusivity of SO_2 in the $CaSO_4$ layer formed during sulfation of CaO particles.

Before we proceed with the investigation of the transient characteristics of the fixed-bed desulfurization reactor and their dependence on the submodels used to model the pore structure evolution process, it would be useful to examine the validity of the pseudosteady state assumption that was used to simplify the model equations and enable us to sequentially solve the three submodels that comprise the overall reactor model. Figure 2 describes the transient response of the H_2S concentration and

Table 1. Physical, Kinetic, Reactor, and Fixed-Bed Data Used for ZnO

$v_S = 14.87 \times 10^{-3}$ m³/kmol	$D_P = 1.5 \times 10^{-12}$ m²/s
$v_P = 24.12 \times 10^{-3}$ m³/kmol	$\epsilon_o = 0.5$
$k_s = 2.5 \times 10^{-5}$ m/s	$\alpha = 1.5$ mm
$T = 700$°C	$x_{H_2S} = 3{,}000$ ppm
$P_e = 500$	$L = 0.1$ m
$u = 0.1$ m/s	$\epsilon_b = 0.3$
$P = 1$ atm	

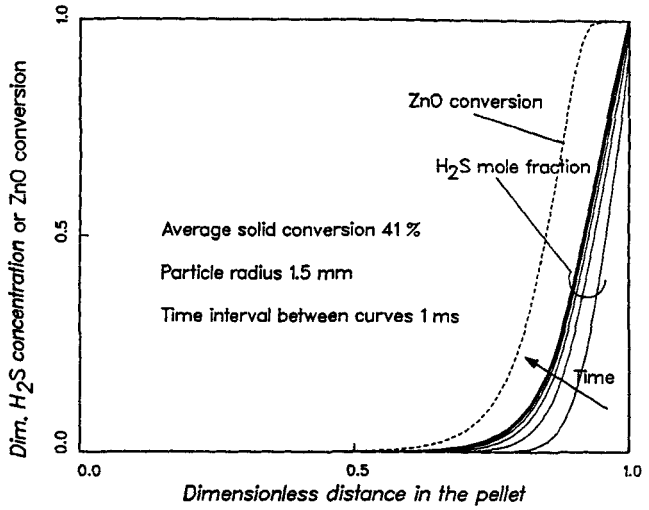

Figure 2. Effects of pseudosteady-state assumption for gaseous species in the interior of pellets.

ZnO conversion profiles, obtained using the transient form of the material balance of hydrogen sulfide in the interior of the pellets (Eq. 8), in a partially reacted (41% average conversion) pellet of ZnO when this is exposed to the reactive mixture at time zero. It is seen that the concentration profile of H_2S reaches steady state in a relatively short time interval (about 4 ms) during which no noticeable change takes place in the conversion profile of the solid (dashed curves). This implies that the employment of the pseudosteady state assumption for the concentration profile of hydrogen sulfide in the pellets will have insignificant effects on the transient behavior of the reactor.

Effects of distribution of pore size

Breakthrough curves for a fixed-bed desulfurization reactor packed with zinc oxide pellets of discrete unimodal or bimodal distribution of pore size are given in Figure 3. The solids of Figure 3 have the same initial porosity and internal surface area but are characterized by different distribution of porosity between small and large pores and different pore sizes. (The initial internal surface area of 1.9×10^7 m^2/m^3 used in the computations corresponds to 7 m^2/g for zinc oxide pellets of porosity 0.5 or to 10 m^2/g for pellets of porosity 0.65.) Using the molar volumes of solid product and solid reactant of Table 1, we find that the stoichiometric molar volume ratio of the ZnO–ZnS system is equal to 1.62. Introducing this value in Eq. 15 shows that complete pore closure can take place only for initial porosities lower than 0.38. Complete utilization is therefore theoretically possible for the solids of Figure 3; it corresponds to about 0.41 g H_2S/g ZnO. The corresponding values of sorbent utilization, expressed as g H_2S/g ZnO, to the results of Figure 3 for 10 ppm breakthrough concentration are shown in Table 2. Notice that approximate values of sorbent utilization for breakthrough concentrations much smaller than the inlet stream concentration can be obtained directly from the breakthrough curves by dividing the breakthrough time by the reaction time for complete sorbent utilization and complete desulfurization of the gas stream (which is equal to about 7.25 days for the reactor and sorbent data of Table 1) and multiplying the result by the maximum sorbent utilization mentioned above.

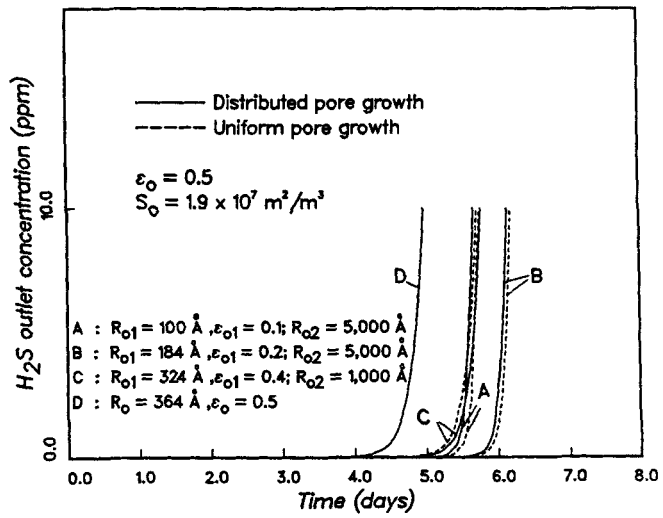

Figure 3. Breakthrough curves for solids with discrete pore-size distribution (unimodal or bimodal) of the same porosity and internal surface area.

The results of Figure 3 and Table 2 indicate that the transient behavior of the reactor, and hence its breakthrough history, is strongly influenced by the type of the pore size distribution of the solid. In order to better understand the behavior of the various curves shown in Figure 3, it is helpful to consider the variation of the local reaction rate constant $k_v(\xi)$ and of the effective diffusivity $D_e(\xi)$ with the local conversion in the interior of the pellets and the variation of the average reaction rate constant $\bar{k}_v(\bar{\xi})$ with the average conversion of the pellets. The respective curves are shown in Figures 4, 5 and 6. As curves D and C of Figure 4 show, introducing large pores in the initial pore structure of the pellets leads, as expected, to higher intraparticle effective diffusivities for all local conversion levels. It also slows down the decrease of the local reactivity of the pellet with the conversion. (See curves D and C of Figure 5.) This behavior is a consequence of the fact that before pore closure starts to take place, the reaction surface area of a distributed pore structure is larger at all porosity levels than that of a unimodal structure of the same initial porosity and internal surface area. (This is always true for uniform pore growth, as it can be shown using Eqs. 29 and 30.) These two effects together lead to higher average reactivities (see Figure 6) for the distributed pore-size solid and, as a result, to larger breakthrough times and higher sorbent utilizations. (Compare cases D and C of Figure 3 and Table 2.)

Increasing the size of the large pores or their contribution to the total initial porosity of the pellets requires that the size of the small pores is decreased in order that the same values of initial

Table 2. Sorbent Utilization (g H_2S adsorbed/g ZnO for the Solids of Figure 3 for 10 ppm Breakthrough Concentration

Solid	Uniform Pore Growth	Distributed Pore Growth
A	0.326	0.321
B	0.35	0.347
C	0.324	0.327
D	0.282	0.282

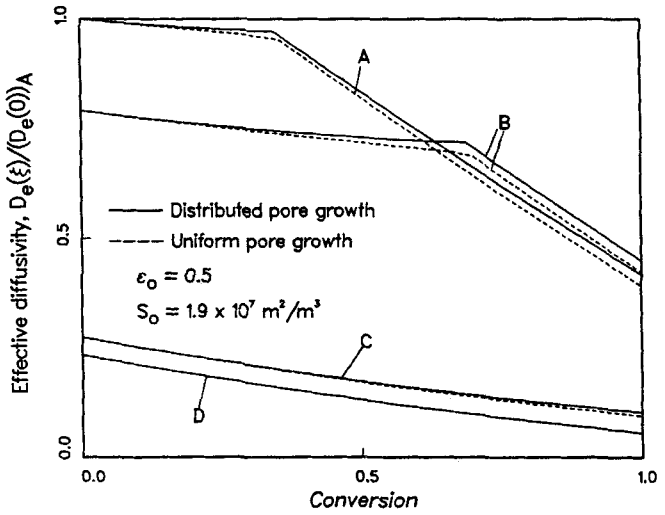

Figure 4. Variation of the effective diffusivity in the pellets of Figure 3 with the local conversion.

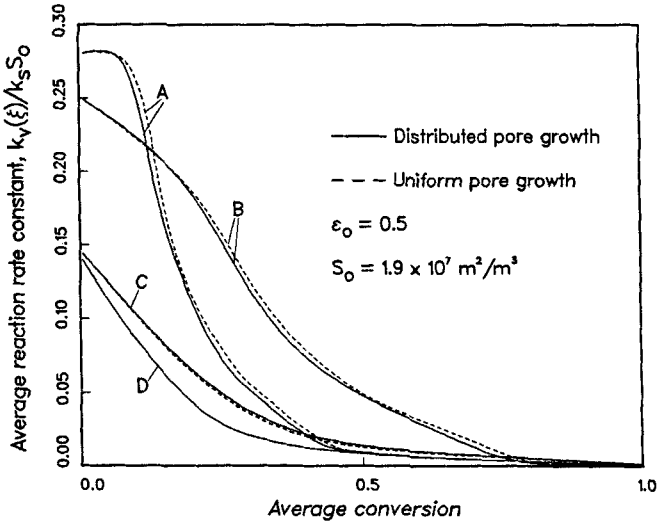

Figure 6. Variation of the average volumetric reaction rate constant in the pellets of Figure 3 with the local conversion in the bed.

surface area and porosity be maintained. The small pores may thus become completely plugged with solid product (since $Z > 1$) before complete conversion is reached, which happens to be the case with solids A and B of Figure 3 and Table 2. It can be shown using Eqs. 20, 24a, and 30 that the value of the conversion at which closure of the small pores takes place in a discrete, bimodal pore structure, ξ^*, is given for uniform pore growth by the expression

$$\xi^* = \frac{1}{Z-1}\left[\frac{(1-\epsilon_{o2})^{(1-R_{o1}/R_{o2})^2}}{1-\epsilon_o} - 1\right] \qquad (47)$$

As Figure 5 shows, when closure of the small pores takes place, the local reactivity of the solid goes through a sharp decrease because the portion of the reaction surface area that is primarily accessed through the small pores ceases to participate in the reaction process. The slope of the effective diffusivity vs. local conversion curve (Figure 4) also goes through an abrupt change

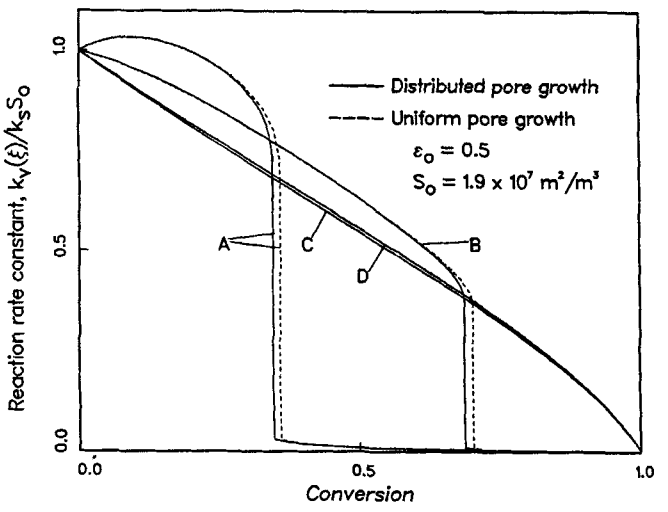

Figure 5. Variation of the volumetric reaction rate constant in the pellets of Figure 3 with the local conversion.

at this conversion level since the conversion now changes only because of reaction in the large pores.

The large drop in the local reaction rate that takes place when the small pores close effects a fast decrease of the average reaction rate of the pellet with the average conversion. (See Figure 6.) It should be pointed out that when concentration gradients exist in the interior of the pellets, closure of the small pores does not take place simultaneously over the entire pellet volume. As a result, no discontinuity appears in the variation of the average reactivity of the pellet with the average conversion. Despite the large drop in the local reaction rate when plugging of the small pores occurs, solid B exhibits the largest breakthrough time. This is not the case for solid A because small pore plugging takes place at a relatively low conversion (about 35%), causing the average reaction rate of pellets A to eventually become lower than that of the other distributed pore size solids (B and C) at about 50% conversion. Thus, notice that the sorbent utilization for solid A is considerably lower than that for solid B, while an analogous observation applies to its breakthrough time.

Figure 3 and Table 2 also demonstrate the effects of the assumption of uniform pore growth on the predictions of the desulfurization model. As Figures 4 and 5 show the assumption of uniform pore growth leads to higher local reactivities but lower intraparticle effective diffusivities. Depending on the relative magnitudes of these effects, their combined action may bring about an increase or a decrease in the average reactivity of the porous solid pellets. (See Figure 6.) The above behavior is due to the fact that when uniform pore growth (or shrinkage) is assumed, the thickness of the product layer that covers the small pores decreases for a given conversion level, while the product layer that covers the large pores becomes thicker. This implies higher local reactivities (which are basically controlled by the small pores) and lower effective diffusivities (which are controlled by the large pores) for solids reacting with uniform pore growth or shrinkage. (See Figures 4 and 5.) For this reason, pore closure takes place at higher conversion levels when the assumption of uniform pore growth is used (cases A and B).

The distributed pore size solid C exhibits insignificant dependence of its local reactivity on the assumption of uniform pore

growth, but its intraparticle diffusivity appears to be influenced noticeably. (See Figures 4 and 5.) As a result, its average reaction rate for uniform pore growth is lower, and its breakthrough times smaller. Cases A and B, on the other hand, present a range of local conversion values, in the vicinity of the point where plugging of the small pores takes place, in which the local reaction rate is considerably higher for uniform pore growth. This eventually leads to higher average reactivities at intermediate and high average conversions (Figure 6) and, therefore, to higher breakthrough times (Figure 3). These observations are in qualitative agreement with conclusions derived from the application of the distributed pore model to limestone sulfation (Sotirchos and Yu, 1985). The effects of uniform or distributed pore growth are rather weak for all four cases considered in Figures 3–6, and consequently, the uniform pore growth structural model may suffice for the study of the overall desulfurization reactor for most pore size distributions. This is a very important conclusion since considerably less numerical effort is required for the solution of the structural model of uniform pore growth; it practically involves the solution of a single ordinary differential equation only.

More results on the effects of the pore size distribution of the solid are presented in Figure 7, which again depicts breakthrough curves for fixed-bed reactors loaded with zinc oxide pellets of discrete, unimodal or bimodal pore size distribution. The initial porosity of the pellets is the same, 0.5, and equally distributed between small and large pores. The radius of the small pores is also the same for all solids, but the radius of the large pores, and consequently the internal surface area, is allowed to vary. Application of Eq. 47 to the distributed pore size solids of Figure 7 shows that solid B does not exhibit small pore closure, while the small pores of solids C and D are completely plugged by solid product at conversions 92 and 86%, respectively. It is seen that the solid with unimodal pore size distribution (A) presents the smallest breakthrough time and, hence, the smallest value of sorbent utilization. This behavior is primarily due to the fact that the resistance for diffusion in the interior of the pellets of solid A is considerably higher than that for the distributed pore size solids (compare with the results of Figure 3). The limitations for mass transport in the pore structure decrease significantly by replacing some of the 400 Å pores with larger (1,000 Å) pores (solid B), and as a result, a marked increase is observed in the breakthrough time in spite of the significant decrease of the internal surface area that accompanies the introduction of larger pores in the structure. The breakthrough time experiences a further increase as the size of the large pores is increased to 5,000 Å, but the solid with large pores of 10,000 Å in radius (solid D) exhibits breakthrough times that are lower than those of the other two solids with distributed pore size (curves B and C). The favorable effect of the decreasing diffusional limitations on the average reactivity of the pellets with increasing size of large pores is offset for solid D by the loss of reaction surface area caused by the plugging of the small pores with solid product.

Typical H_2S concentration and ZnO conversion profiles in the fixed bed are presented in Figures 8 and 9 at time intervals of 1 day. The profiles shown in Figure 8 are for a fixed bed loaded with pellets having discrete, bimodal pore size distribution (solid B of Figure 3), while those given in Figure 9 are for pellets with unimodal distribution of pore size (solid D of Figure 3). As it was pointed out during the discussion of the results of Figures 3–6, the small pores of the pellets of solid B are completely plugged with solid product at about 70% local conversion causing a significant drop in the local and average reactivity of the pellets at about the same value of local and average conversion. (See Figures 5 and 6.) This is exactly the reason for which the conversion profiles in the bed (solid curves of Figure 8) tend to level off at about 70% conversion. The bed with unimodal distribution of pore size (Figure 9), on the other hand, is characterized by less steep profiles, which explain its smaller breakthrough times (Figure 3). Recall that although the pellets with unimodal pore size distribution do not undergo pore closure, they are characterized by very low average reaction rates—because of strong intraparticle diffusional limitations (see Figures 4 and 6). As the results of Figure 6 show, the pellets of solid D (Figure 9) present higher reaction rates than the pellets of solid B (Figure 8) for conversion higher than 75%. Indeed, as a comparison of Figures 8 and 9 reveals, the bed with pellets D attains higher conversions at the entrance of the reactor at large

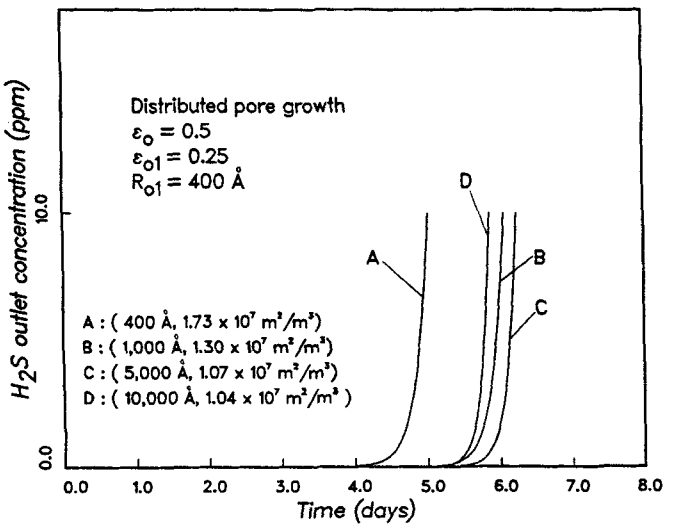

Figure 7. Breakthrough curves for solids with discrete pore size distribution (unimodal or bimodal).

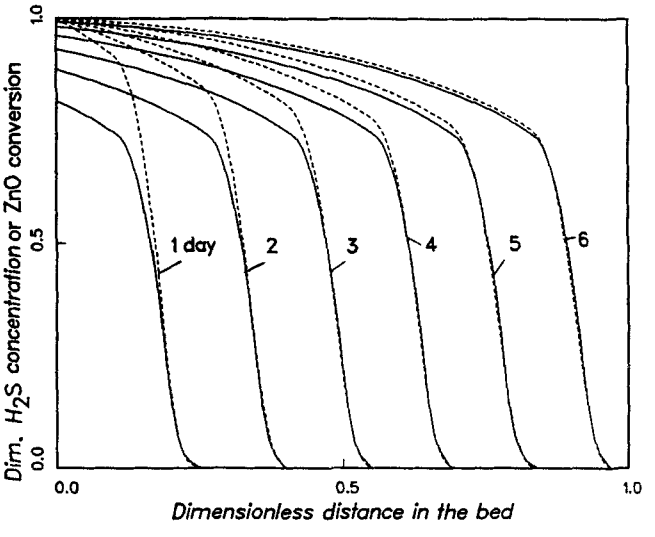

Figure 8. Concentration and conversion profiles in the reactor for solid B of Figure 3.

—, solid conversion; ---, H_2S concentration.

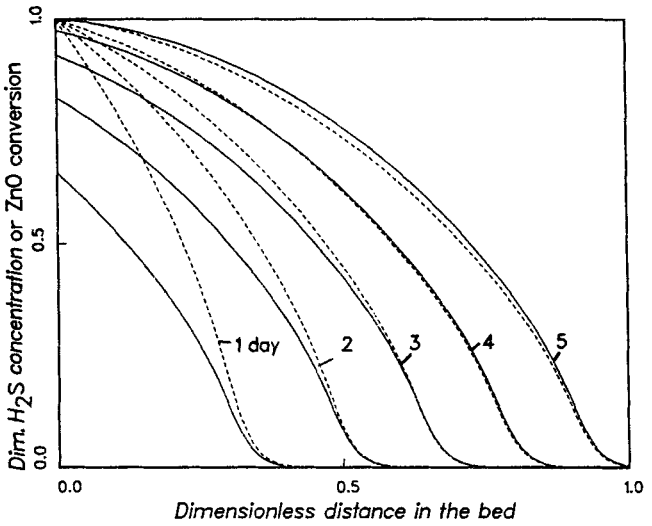

Figure 9. Concentration and conversion profiles in the reactor for solid D of Figure 3.

—, solid conversion, ---, H_2S concentration.

exposure times (greater than 3 days), but this fact cannot counterbalance the effects of lower conversions in the rest of the fixed-bed reactor.

Effects of distribution of grain size

We now turn our attention to the investigation of the effects of the grain size distribution of the solid and of the assumption of uniform grain growth (or shrinkage) on the predictions of the fixed-bed desulfurization model. Breakthrough curves for fixed beds loaded with pellets of discrete, unimodal or bimodal grain size distribution (spherical grains) are given in Figure 10. The three grain structures used in the figure have the same initial porosity and internal surface area, equal to those of the pore structures of Figure 3. The variation of the local reactivity of the solids, expressed in terms of the volumetric reaction rate constant $k_v(\xi)$, with the local conversion is shown in Figure 11. The breakthrough behavior of the reactor appears to be strongly influenced by the grain size distribution of the solid. In contrast with the results for pore structures (Figure 3) where the breakthrough time of the fixed bed loaded with pellets of uniform pore size is the smallest, the solid with unimodal grain size distribution presents the greatest breakthrough time. The two types of porous structures behave differently mainly because the reaction surface area of a distributed grain structure is smaller at conversions greater than zero than that of a unimodal grain structure of the same initial porosity and internal surface area while, as mentioned before, the opposite is true for pore structures. For the same reason the local reactivity of distributed grain structures (see Figure 11) is smaller than the reactivity of the uniform grain size solid. It should be pointed out that the solids with distributed grain size are also characterized by smaller effective diffusivities at nonzero conversions, a result of their larger pore surface areas. (See Eq. 43.)

The unreacted core of the small grains vanishes before complete (local) conversion is reached. The variation of the local reactivity with the conversion presents a discontinuity in its slope at the point where this happens. (See Figure 11.) It can be shown using Eqs. 23, 24a, and 32 that the unreacted core of the small grains in a discrete, bimodal grain structure vanishes at conversion ξ^* given for uniform grain growth by the expression (for $R_{o1} \leq R_{o2}$)

$$\xi^* = \frac{(1 - \phi_{o2})^{(1-R_{o1}/R_{o2})^{z+1}} - \epsilon_o}{1 - \epsilon_o} \tag{48}$$

which predicts 60% and 82% conversion for solids A and B of Figures 10 and 11. As seen in Figure 11, the assumption of uniform grain growth delays the disappearance of the unreacted core of the small grains and leads to higher local reactivities, a result of higher surface areas. Despite this, however, the fixed beds loaded with pellets reacting with uniform grain growth present smaller breakthrough times. This is caused by the smaller diffusivities of the uniformly reacting grain structures which counterbalance the influence of the higher volumetric

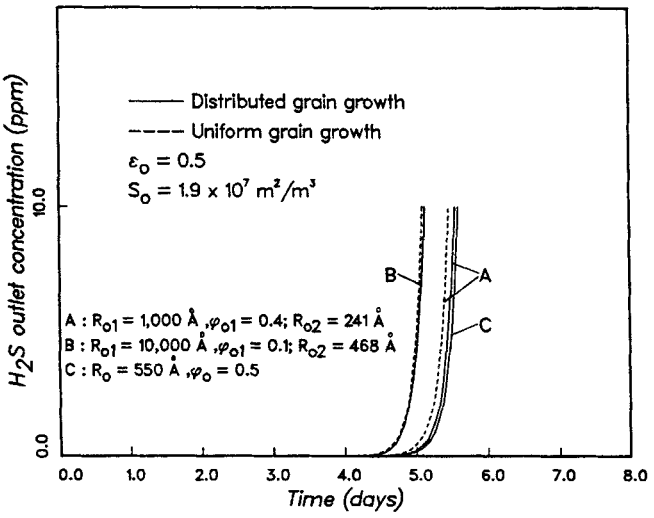

Figure 10. Breakthrough curves for solids with discrete grain-size distribution (unimodal or bimodal) of the same porosity and internal surface area.

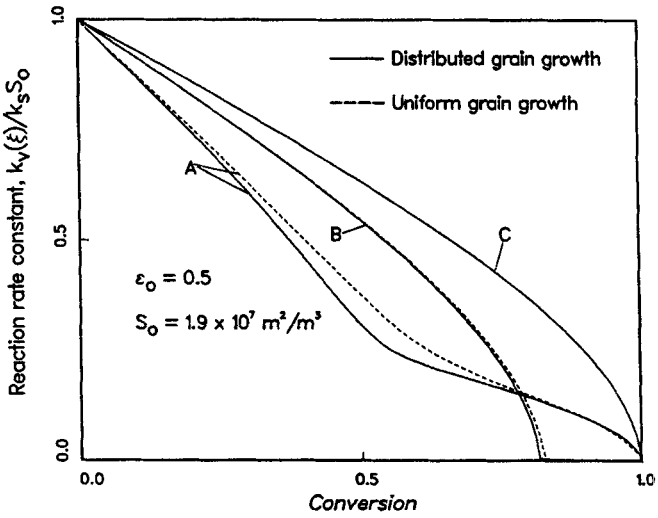

Figure 11. Variation of the volumetric reaction rate constant in the pellets of Figure 10 with the local conversion.

reaction rate constants (Figure 11). Because of these two antagonistic factors, the effects of the assumption of uniform grain growth on the transient behavior of the desulfurization reactor were found to be weak for all grain size distributions considered. It can thus be argued that the much simpler structural model for uniformly reacting grain structures may satisfactorily be employed to describe the structural evolution of the pellets of the sorbent.

Acknowledgment

This work has been supported by a grant from the U.S. Dept. of Energy.

Notation

a = radius of the particle, m
c = concentration of the reactant gas, kmol/m^3
D_e = effective diffusion coefficient in the pellet, m^2/s
D_P = diffusion coefficient in the product layer, m^2/s
D_b = axial dispersion coefficient in the bed, m^2/s
D_A = diffusion coefficient of gaseous reactant in a pore, m^2/s
D_{KA} = Knudsen diffusion coefficient in a pore, m^2/s
$\mathcal{D}_{AB}$ = bulk diffusion coefficient of gaseous reactant, m^2/s
g_i = auxiliary variables defined in Eq. 27, m
k_g = mass transfer coefficient, m/s
k_v = local volumetric reaction rate constant (in the pellet), s^{-1}
$\bar{k}_v$ = local volumetric reaction rate constant (in the bed), s^{-1}
$l(R)dR$ = length per unit volume of axes of pores with radius in the range $[R, R + dr]$, m/m^3
L = length of the fixed bed, m
$n(R)dR$ = number per unit volume of grains with size in the range $[R, R + dr]$, m^{-3}
Pe = Peclet number ($\mu L/D_e$)
q = uniform growth or shrinkage variable, m
r = radial distance in a pellet, m
R = capillary or grain radius, m
R_o = grain size or radius at time $t = 0$, m
R_v = average local reaction rate, per unit volume, kmol/m^3 · s
$\bar{R}_v$ = average local reaction rate in the bed, per unit of pellet volume, kmol/m^3 · s
S = internal surface area of a two-phase structure (m^2/m^3)
Sh = Sherwood number ($Sh = k_g a/D_e$)
t = time, s
v_i = specific molar volume of solid i, m^3/kmol
z = axial distance in the bed, m
Z = stoichiometric volume ratio (v_P/v_S)

Greek letters

ϵ = porosity of a capillary or grain structure
$\epsilon(R)dR$ = porosity due to pores with radius in the range $[R, R + dR]$
η = tortuosity factor
ν_b = stoichiometric coefficient of the gas
ξ = local conversion in the pellets
$\bar{\xi}$ = average conversion of the pellets or local conversion in the bed
ϕ = volume fraction of the solid phase

Subscripts

$1, \ldots, N$ = refer to the ith pore or grain size of a discrete distribution
f = refers to the gas phase in the bed
o = refers to $t = 0$
p = refers to the pore surface or to the pore space
P = refers to the solid product
r = refers to the reaction surface
S = refers to the solid reactant

Literature Cited

Anderson, G. L., F. O. Berry, and M. N. Gross, "Development of a Hot Gas Cleanup System for Integrated Coal Gasification/Molten Carbonate Fuel Cell Power Plants," Topical Report, DOE/MC/19403-1544 (1984).

Burganos, V. N., PhD Diss., Univ. of Rochester, Rochester, NY (1988).

Christman, P. G., and T. F. Edgar, "Distributed Pore-Size Model for the Sulfation of Limestone," *AIChE J.*, **29**, 388 (1983).

Danckwerts, P. V., "Continuous Flow Systems," *Chem. Eng. Sci.*, **2**, 1 (1953).

de Boor, C., *A Practical Guide to Splines*, Springer-Verlag, New York (1978).

Froment, G. F., and K. B. Bischoff, *Chemical Reactor Analysis and Design*, Wiley, New York (1979).

Gaillet, D. A., and D. P. Harrison, "Structural Property Variations in the MnO-MnS System," *Chem. Eng. Sci.*, **37**, 625 (1982).

Gavalas, G. R., "A Random Capillary Model with Application to Char Gasification at Chemically Controlled Rates," *AIChE J.*, **26**, 577 (1980).

Gibson, J. B., and D. P. Harrison, "The Reaction between Hydrogen Sulfide and Spherical Pellets of Zinc Oxide," *Ind. Eng. Chem. Process Des. Dev.*, **19**, 231 (1980).

Jalan, V., "Studies Involving High Temperature Desulfurization/Regeneration Reactions of Metal Oxides for Fuel Cell Development," Final Report, DOE/MC/16021-1486 (1983).

Lee, H. H., *Heterogeneous Reactor Design*, Butterworth, Boston (1985).

Ranade, P. V., and D. P. Harrison, "The Variable Property Grain Model Applied to the Zinc Oxide-Hydrogen Sulfide Reaction," *Chem. Eng. Sci.*, **36**, 1079 (1981).

Sotirchos, S. V., and H. C. Yu, "Mathematical Modelling of Gas-Solid Reactions with Solid Product," *Chem. Eng. Sci.*, **40**, 2039 (1985).

Sotirchos, S. V., and H. C. Yu, "Overlapping Grain Models for Gas-Solid Systems with Solid Product," *Ind. Eng. Chem. Res.*, **27**, 836 (1988).

Tamhankar, S. S., "Studies on the Regeneration of Sulfided Iron Oxide Sorbent with Steam-Air Mixtures," Final Report, DOE/MC/16022-1307 (1982).

Tamhankar, S. S., M. Hasatani, and C. Y. Wen, "Kinetic Studies on the Reactions Involved in the Hot Gas Desulfurization Using a Regenerable Iron Oxide Sorbent: I. Reduction and Sulfidation of Iron Oxide," *Chem. Eng. Sci.*, **36**, 1181 (1981).

Westmoreland, P. R., J. B. Gibson, and D. P. Harrison, "Comparative Kinetics of High-Temperature Reaction between H_2S and Selected Metal Oxides," *Environ. Sci. Technol.*, **11**, 488 (1977).

Yu, H. C., and S. V. Sotirchos, "A Generalized Pore Model for Gas-Solid Reactions Exhibiting Pore Closure," *AIChE J.*, **33**, 382 (1987).

Manuscript received July 13, 1988, and revision received Mar. 21, 1989.